*Inorg. Chem.* **2003**, *42*, 4650–4659

# Magic Electron Counts and Bonding in Tubular Boranes

**Musiri M. Balakrishnarajan,[†] Roald Hoffmann,*[,†] Pattath D. Pancharatna,[‡] and Eluvathingal D. Jemmis*[,‡]**

*Department of Chemistry and Biochemistry, Cornell University, Ithaca, New York 14853, and School of Chemistry, University of Hyderabad, Hyderabad, India 500 046*

Received December 6, 2002

Ring stacking in some *closo*-borane dianions and the hypothetical capped borane nanotubes, predicted to be stable earlier, is analyzed in a perturbation theoretic way. A "staggered" building up of rings to form nanotubes is explored for four- and five-membered $B_nH_n$ rings. Arguments are given for the stacking of $B_5H_5$ rings being energetically more favorable than the stacking of $B_4H_4$ rings. Elongated B–B distances in the central rings are predicted for some nanotubes, and the necessity to optimize ring–cap bonding is found to be responsible for this elongation. This effect reaches a maximum in $B_{17}H_{17}^{2-}$; the insertion of additional rings will reduce this elongation. These *closo*-borane nanotubes obey Wade's $n + 1$ rule, but the traditional explanation based on a partitioning into radial/tangential molecular orbitals is wanting.

## 1. Introduction

Boron exhibits a wide variety of polyhedral frameworks in boranes and boron-rich solids, ranging from highly symmetric octahedra and icosahedra to quite open and unsymmetrical skeletons. Following a variety of theoretical approaches including resonance theory[1] and molecular orbital theory,[2] and a general formulation by Lipscomb and others[3] of electron deficient multicenter bonding for boranes, a major breakthrough in our qualitative understanding of these systems was achieved in the early 1970s by the formulation of Wade's rule.[4] This rule provides the electronic requirements of a given *closo* polyhedral skeleton as $n + 1$ electron pairs, where $n$ is the total number of vertices. Wade's rule is derived from empirical observations and preceding theoretical calculations[2,3] for $n$-vertex *closo* polyhedra, and has some well-known exceptions.[5] With its ability for extension to *nido* and the more open *arachno* systems, Wade's rule has enjoyed huge success in rationalizing the diverse structural patterns exhibited by polyhedral boranes, and in predicting new structures.

While the origin of the rule was empirical, Wade gave a justification based on molecular orbital theory as follows: The boron atoms in a generalized $n$-vertex polyhedron are assumed to exhibit sp hybridization, with an sp hybrid radiating away from the center of the cage used for a 2c−2e bond to a hydrogen or an external ligand. This leaves one *radial* sp hybrid and two unhybridized *tangential* p orbitals for skeletal bonding. Taking octahedral $B_6H_6^{2-}$ for illustration,[6] Wade reasoned that from the set of $n$ radial sp hybrids that point toward the center only one strongly bonding molecular orbital is formed; the rest of the radial MOs were taken as antibonding. The $2n$ tangential p orbitals form $n$ bonding and $n$ antibonding skeletal orbitals, resulting in a total of $n + 1$ bonding molecular orbitals (BMO). This generalization is assumed to hold for all *closo* polyhedra. Some stabilization due to the mixing of the higher lying out-of-phase combinations of radial MOs with the tangential BMOs is anticipated, but this is not expected to affect the general conclusion.

Initial attempts to justify Wade's rule employed graph theory;[7] the presence of the single bonding radial orbital was correlated with the unique positive eigenvalue of the

* Authors to whom correspondence should be addressed. E-mail: rh34@cornell.edu (R.H.); jemmis@uohyd.ernet.in (E.D.J.).

† Cornell University.

‡ University of Hyderabad.

(1) Lipscomb, W. N. *Boron Hydrides*; Benjamin: New York, 1963.

(2) (a) Longuet-Higgins, H. C.; Roberts, M. de V. *Proc. R. Soc. London, Ser. A* **1955**, *230*, 110. (b) Longuet-Higgins, H. C.; Roberts, M. de V. *Proc. R. Soc. London, Ser. A* **1954**, *224*, 336. (c) Longuet-Higgins, H. C. *Q. Rev., Chem. Soc.* **1957**, *11*, 121.

(3) Hoffmann, R.; Lipscomb, W. N. *J. Chem. Phys.* **1962**, *36*, 2179.

(4) (a) Wade, K. *J. Chem. Soc. D* **1971**, 792. (b) Wade, K. *Adv. Inorg. Chem. Radiochem.* **1976**, *18*, 1.

(5) (a) Stone, A. J.; Alderton, M. J. *Inorg. Chem.* **1982**, *21*, 2297. (b) Fowler, P. W. *Polyhedron* **1985**, *4*, 2051.

(6) (a) Albright, T. A.; Burdett, J. K.; Whangbo, M. *Orbital Interactions in Chemistry*; John Wiley & Sons, Inc.: New York, 1985; Chapter 22. (b) Fox, M. A.; Wade, K. In *The Borane, Carborane, Carbocation Continuum*; Casanova, J., Ed.; John Wiley & Sons, Inc.: New York, 1998; p 57.



10.1021/ic0262435 CCC: $25.00 
Published on Web 06/20/2003

complete graph of $n$ vertices, but it failed to explain the exceptions. Later, Stone's study of *closo* boranes[5,8] ($n$ = 4−12), using a surface harmonics model, characterized the exceptions that occurred for $B_4H_4$ ($T_d$), and $B_{14}H_{14}^{2-}$ ($T_d$), where the number of bonding tangential orbitals is found to be one more or less than $n$ as a consequence of symmetry. Despite lingering doubts about the existence of a single radial BMO,[6a] this is tacitly assumed in all these approaches. The nature of mixing between the tangential and radial MOs remains largely unexplored. Among the *closo* systems, octahedra and icosahedra are ubiquitous in boron-rich solids,[9] though other structures[10] are also known.

Earlier MO calculations on polyhedral boranes involved in the development of extended Hückel theory[3] were followed by HF-SCF calculations.[11] Since then many experimental and hypothetical $B_nH_n^{2-}$ systems ($n$ = 4−17) were characterized at several levels of theory,[12] and the stable isomers and their geometries were reported. But the underlying reasons for the geometries and stabilities have been afforded only a cursory view using topology-based arguments. Understanding the multicentered bonding in these systems remains a challenge.

As a part of our approach to a general theory of boron hydrides,[13] in this report we present a systematic perturbation theory based molecular orbital investigation of the effect of stacking four- and five-membered boron rings. The nature of all the BMOs, which are mainly responsible for polyhedral bonding, is investigated. These molecular orbitals are conveniently derived by using the starting point of the radial sp hybrid and the two tangential p orbitals mentioned earlier. For simplicity, other MOs that are primarily B−H bonding and those lying in the antibonding region are excluded. This choice avoids the complications of mixing of the *exo* bonding and antibonding MOs (really present but less important) that have the same symmetries as the $n$ radial sp hybrids. The energies of the MOs for the molecules as well as those of fragments, that we will use, derive from extended Hückel calculations[3,14] with the experimental distances found in the respective *closo* boranes; ab initio calculations also give the same ordering of levels for all the selected systems.

Beginning with the well-studied $B_6H_6^{2-}$ and $B_7H_7^{2-}$ to illustrate ring−cap interactions, we proceed to stacked systems by exploring the experimentally characterized $B_{10}H_{10}^{2-}$ and $B_{12}H_{12}^{2-}$ and the as yet hypothetical $B_{17}H_{17}^{2-}$, $B_{22}H_{22}^{2-}$, and $B_{27}H_{27}^{2-}$. The equilibrium B−B bond lengths for these dianions (illustrated in Figure 1) were calculated by us from density functional theory (DFT) optimizations using the Gaussian 98 suite of programs[16] at the density functional based B3LYP/6-31G* level of theory,[17] which reproduces the experimental geometry of known boranes well.[11] The smaller species (all except $B_{22}H_{22}^{2-}$ and $B_{27}H_{27}^{2-}$) had been calculated at this level earlier.[11]

Our aim is a detailed understanding of the general nature of bonding in these polyhedra, the derivation of a general electron counting rule for the larger systems, and an explanation of the geometrical details for these systems. The focus is on how the symmetry dictates the nature of orbital interactions and consequently the geometry and bonding in these systems, with special emphasis on the effect of "staggered stacking" of borocyclic rings.[18]

## 2. Intermolecular Interaction of Ring and the Cap Fragments

The formation of the orbitals of $B_6H_6^{2-}$ and $B_7H_7^{2-}$ from fragments is a good introduction to our analytical process. The molecular orbitals of $B_6H_6^{2-}$ can be constructed from the orbitals of a cyclobutadienoid square $B_4H_4^{6-}$ ring[6a] ($D_{4h}$) and those of two $B-H^{2+}$ caps, as shown in Figure 2.

The charge assignment in the fragments is, of course, arbitrary. To simplify the diagram, we have tentatively ignored antibonding MOs of the $B_4H_4^{6-}$ fragment. The interaction between the fragments shown in Figure 2 leads to one strongly bonding radial MO of $a_{1g}$ symmetry and two sets of triply degenerate orbitals (the $O_h$ symmetry forces these degeneracies). The low-lying $t_{1u}$ set has the out-of-phase combination of the cap sp hybrids interacting with the p orbitals directed toward them. It is interesting to note that radial−tangential mixing enters even in this simple molecule. The next higher $t_{2g}$ set is made up purely of unhybridized tangential p orbitals of boron, free from any mixing of sp hybrids. It forms the HOMO (highest occupied MO). In accord with Wade's simplified explanation, there are one strongly bonding *radial* orbital ($a_{1g}$) and six BMOs ($t_{1u}$ and $t_{2g}$) that are mainly *tangential* in character.


(7) King, R. B.; Rouvray, D. H. *J. Am. Chem. Soc*. **1977**, *99*, 7834.
(8) (a) Stone, A. J. *Mol. Phys.* **1980**, *41*, 1339. (b) Stone, A. J. *Inorg. Chem.* **1981**, *20*, 563.
(9) Emin, D.; Aselage, J.; Beckel, C. L.; Howard, I. A.; Wood, C. *Boron Rich Solids*; AIP Conference Proceedings 231; American Institute of Physics: New York, 1994.
(10) Albert, B. *Eur. J. Inorg. Chem*. **2000**, 1679.
(11) (a) Schleyer, P. v. R.; Najafian, K.; Mebel, A. M. *Inorg. Chem*. **1998**, *37*, 6765. (b) McKee, M. L.; Wang, Z.; Schleyer, P. v. R. *J. Am. Chem. Soc*. **2000**, *122*, 4781.
(12) Schleyer, P. v. R.; Najafian, K. In *The Borane, Carborane, Carbocation Continuum*, Casanova, J., Ed.; John Wiley & Sons, Inc.: New York, 1998; p 169.
(13) (a) Jemmis, E. D.; Balakrishnarajan, M. M.; Pancharatna, P. D. *Chem. Rev.* **2002**, *102*, 93. (b) Balakrishnarajan, M. M.; Jemmis, E. D. *J. Am. Chem. Soc*. **2000**, *122*, 4516. (c) Jemmis, E. D.; Balakrishnarajan, M. M.; Pancharatna, P. D. *J. Am. Chem. Soc.* **2001**, *123*, 4313.
(14) Hoffmann, R. *J. Chem. Phys*. **1963**, *39*, 1397.
(15) (a) Jemmis, E. D. *J. Am. Chem. Soc.* **1982**, *104*, 7017. (b) Jemmis, E. D.; Schleyer, P. v. R. *J. Am. Chem. Soc.* **1982**, *104*, 4781. (c) Jemmis, E. D.; Pavankumar, P. N. V. *Proc.—Indian Acad. Sci., Chem. Sci.* **1984**, *93*, 479. (d) Jemmis, E. D.; Balakrishnarajan, M. M. *Bull. Mater. Sci*. **1999**, *22*, 101.
(16) Frisch, M. J.; Trucks, G. W.; Schlegel, H. B.; Gill, P. M. W.; Johnson, B. G.; Robb, M. A.; Cheeseman, J. R.; Keith, T.; Peterson, G. A.; Montgomery, J. A.; Raghavachari, K.; Al-Laham, M. A.; Zakrzewski, V. G.; Oritz, J. V.; Foresman, J. B.; Cioslowsky, J.; Stefenov, B. B.; Nanayakkara, A.; Callacombe, M.; Peng, C. Y.; Ayala, P. Y.; Chen, W.; Wong, M. W.; Andres, J. L.; Replogle, E. S.; Gomberts, R.; Martin, R. L.; Fox, D. J.; Binkley, J. S.; Defrees, D. J.; Baker, J.; Stewart, J. P.; Head-Gordon, M.; Gonzalez, C.; Pople, J. A. *Gaussian 98*, version 5.2; Gaussian Inc.: Pittsburgh, PA, 1995.
(17) B3LYP is Becke's three parameter hybrid method with LYP correlation functional: (a) Becke, A. D. *J. Chem. Phys.* **1993**, *98*, 5648. (b) Lee, C.; Yang, W.; Parr, R. G. *Phys. Rev. B* **1988**, *37*, 785. (c) Vosko, S. H.; Wilk, L.; Nusair, M. *Can. J. Phys.* **1980**, *58*, 1200. (d) Stephens, P. J.; Delvin, F. J.; Chabalowski, C. F.; Frisch, M. J. *J. Phys. Chem*. **1994**, *98*, 11623.
(18) (a) Brown, L. D.; Lipscomb, W. N. *Inorg. Chem*. **1977**, *16*, 2989. (b) Gindulyte, A.; Lipscomb, W. N.; Massa, L. *Inorg. Chem*. **1998**, *37*, 6544. (c) Sabra, M. K.; Boustani, I. *Europhys. Lett.* **1998**, *42*, 611.

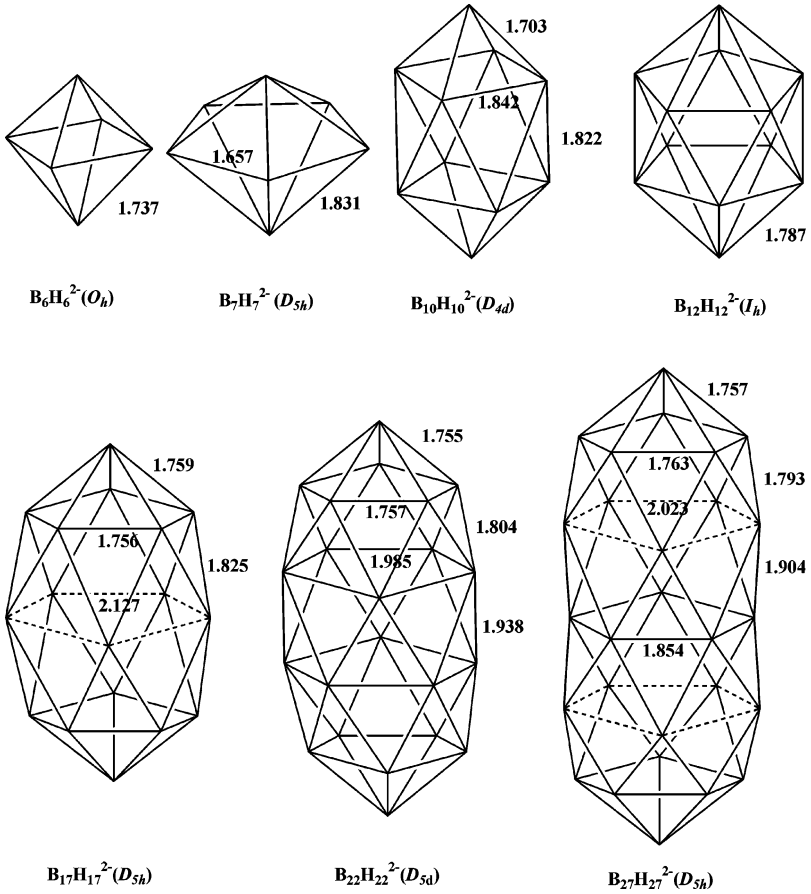


**Figure 1.** Monocage *closo* boranes with bond lengths (in Å) as calculated at the B3LYP/6-31G* level of theory. The hydrogens are omitted for clarity.

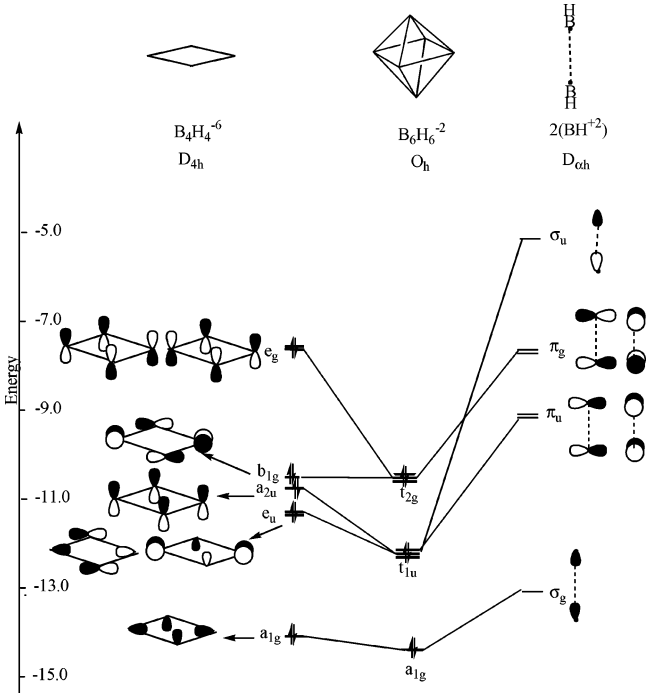


**Figure 2.** The interaction diagram between an *arachno*-$B_4H_4^{6-}$ fragment with two $BH^{2+}$ caps, resulting in the BMOs of *closo*-$B_6H_6^{2-}$.

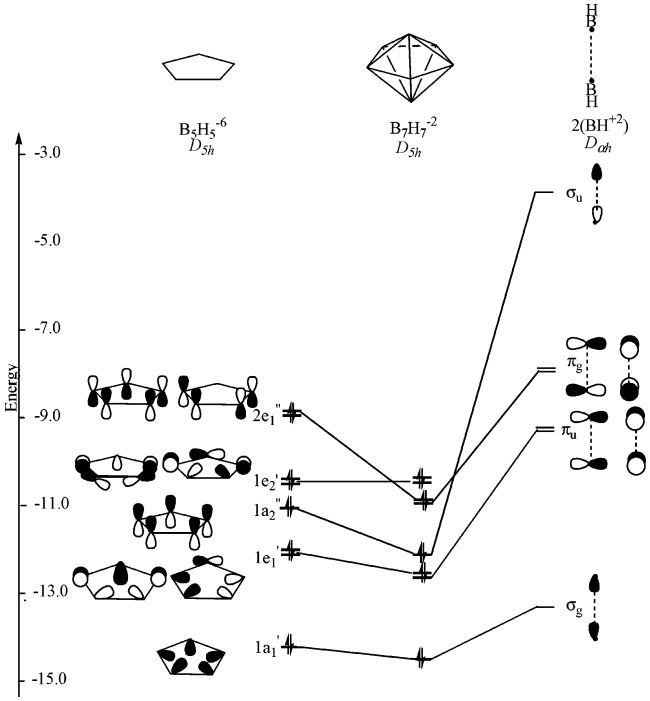


**Figure 3.** The interaction diagram between an *arachno*-$B_5H_5^{6-}$ fragment with two $BH^{2+}$ caps resulting in the BMOs of *closo*-$B_7H_7^{2-}$.

The orbitals of $B_7H_7^{2-}$ can be constructed in an exactly analogous way by the interaction of two $B-H^{2+}$ caps with the five-membered $B_5H_5^{6-}$ ring, as in Figure 3. As predicted by Wade's rule, this interaction produces seven tangential BMOs (bonding MOs) and one totally symmetric $a_1$ radial orbital. The $1e_1'$ MO of the ring interacts with the two bonding combination of cap orbitals, whereas the all-bonding perpendicular $p_z$ ($\pi$) set of the ring ($1a_2''$) interacts with the

out-of-phase combination of the two cap sp hybrids that are of the same symmetry. However, the degenerate set of high-lying $\sigma$ orbitals of the ring ($1e_2'$ in symmetry) find no matching orbitals from the B−H group and form the HOMO. The $2e_1''$ $\pi$ set is similar to the HOMO of the cyclopentadiene ($C_5H_5^-$) ring. This MO has a nodal plane; it interacts strongly with the out-of-phase combination of the cap p orbitals and hence is pushed below $1e_2'$.

In order to assess the effectiveness of the interaction of the B−H group with four- and five-membered rings,[19] we calculated the group Mulliken overlap population (group-OP) of all the molecular orbitals of one B−H group with the bonding molecular orbitals of the $B_4H_4^{6-}$ and $B_5H_5^{6-}$ rings, keeping the B−B bond lengths fixed at an ideal distance of 1.75 Å. The group-OP of the B−H cap with the four- and five-membered rings are found to be 1.85 and 1.76, respectively. The group-OP increases from 1.76 to 1.80 when the hydrogens of the ring in *nido*-$B_6H_6^{4-}$ ($B_5H_5^{6-}$ + $BH^{2+}$) are bent toward the cap by 15.6°. This is the optimum angle obtained by following the extended Hückel total energies as a function of the angle of bending. At the MNDO level, this value is reported to be increased to 17.4°.[15c] An energy minimum is also obtained for $B_5H_5^{4-}$ ($B_4H_4^{6-}$ + $BH^{2+}$) at a bending angle of 6.4°; here the group-OP is maintained as 1.85. This indicates that, irrespective of hydrogen bending, the $B_4H_4^{6-}$ ring is more effective at bonding with the capping B−H group.

The introduction of one more cap perturbs the hydrogen atoms as they are driven by symmetry to come into the plane of the central ring. Presumably, the overlap between the ring orbitals and those of the caps is greater in $B_6H_6^{2-}$ than in $B_7H_7^{2-}$. The resultant group-OPs are 4.05 and 3.61, respectively.

But is the overlap between the various FMOs (fragment MOs) of the pentagonal ring and the caps optimal? We probed this point by changing one important remaining geometrical parameter, the ring B−B distances. A reduction in the ring B−B distances of the five-membered ring to the B3LYP/6-31G* optimized distance of 1.657 Å increases the stabilization due to bicapping to 5.25 eV. Even with this pronounced difference in "capping" and "equatorial" (ring) distances, the stabilization due to capping B−H groups is less than for $B_6H_6^{2-}$ by 2.62 eV. The B−H caps stabilize the $B_4H_4^{6-}$ ring orbitals by 7.87 eV, whereas the stabilization is only 5.25 eV for $B_5H_5^{6-}$. Though it is not easy to compare the stability of two molecules of different stoichiometry, and the distribution of known structures is not a certain guide to stability, we think that the results point to a special stability for $B_6H_6^{2-}$. This is consistent with the earlier observations and the abundance of octahedral $B_6$ units in boron-rich solids.

Replacement of one of the BH caps in $B_6H_6^{2-}$ and $B_7H_7^{2-}$ by a *nido*-$B_5H_5$ and *nido*-$B_6H_6$, respectively, in a staggered fashion, leads to $B_{10}H_{10}^{2-}$ and $B_{12}H_{12}^{2-}$. As the ring B−H bonds of these fragments are no longer required to be in the plane of the ring by symmetry, they tilt toward the caps. In the next two sections, the nature of these interactions is analyzed systematically using the standard tools of perturbation theory. We first look at the intermolecular perturbation of two staggered *nido* fragments keeping the B−H bonds in the plane of the ring, and then proceed to study the effect of geometrical perturbation due to the bending of ring B−H bonds.

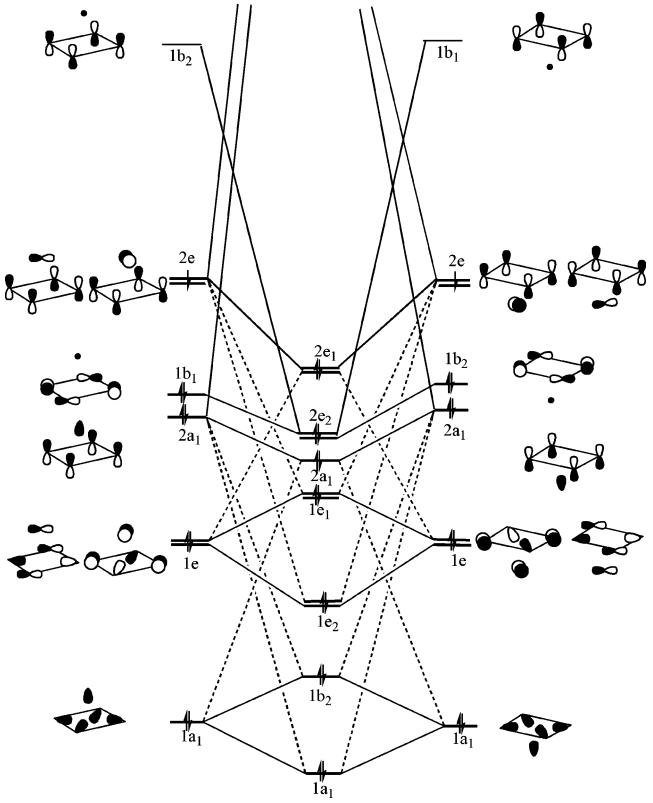


**Figure 4.** The interaction diagram between two *nido*-$B_5H_5^-$ fragments resulting in the bonding MOs of *closo*-$B_{10}H_{10}^{2-}$. Here dashed lines indicate second-order interactions.

## 3. Intermolecular Interaction of Two Staggered *Nido* Fragments

The molecular orbitals of $B_{10}H_{10}^{2-}$ can be conveniently analyzed by the interaction of its two $B_5H_5^{4-}$ ($C_{4v}$) fragments arranged in a staggered fashion. The resulting interaction diagram is illustrated in Figure 4. Here, the ordering of energy levels (while schematic in nature) is derived from extended Hückel calculations using the bond lengths taken from the optimized geometry of $B_{10}H_{10}^{2-}$ at the B3LYP/6-31G* level of theory, but keeping the B−H bonds in the plane of the $B_4H_4$ ring. There is a complication in the group theory here, which is a consequence of the general convention employed in $C_{4v}$ to choose $\sigma_d$ planes as passing through the atoms of the four-membered ring and $\sigma_v$ to pass between them. In the $D_{4d}$ symmetry of $B_{10}H_{10}^{2-}$, such a choice is impossible to maintain simultaneously for both fragments. This problem affects only the assignment of symmetry labels to $b_1$ and $b_2$ orbitals. (The choice we made here is to have an absolute coordinate system in $D_{4d}$, which then has $\sigma_d$ through the atoms for the left hand side $B_5H_5$ fragment in Figure 4 and between them in the right hand side.)

(19) (a) Underwood, D. J.; Hoffmann, R.; Tatsumi, K.; Nakamura, A.; Yamamato, Y. *J. Am. Chem. Soc.* **1985**, *107*, 5968. (b) Clark, H. C.; Jain, V. K. *Coord. Chem. Rev.* **1984**, *55*, 151.

The totally symmetric radial MOs ($1a_1$) of the two fragments interact, in a typically destabilizing two-orbital−four-electron interaction. However, the higher lying FMOs ($2a_1$)—the all-bonding combination of perpendicular $p_z$ orbitals of the ring and sp hybrids of the caps—generate orbitals of the same symmetry in the composite molecule. This leads to second-order interactions by which both the out-of-phase combination ($1b_2$) and in-phase combination ($1a_1$) are stabilized. The out-of-phase combination $1b_2$ remains deep inside the bonding region. Hence, contrary to the single radial orbital observed in $B_6H_6^{2-}$ and $B_5H_5^{2-}$, in $B_{10}H_{10}^{2-}$ two radial MOs are occupied. A similar effect is observed with the interaction of the next degenerate 1e set, as both in-phase and out-of-phase combinations remain within the bonding region of $B_{10}H_{10}^{2-}$, due to stabilizing second-order mixing of the 2e orbitals. The perpendicular $p_z$ orbitals of $2a_1$, as mentioned above, interact particularly strongly with each other. As a result, their out-of-phase ($b_2$) combination is pushed up high into the antibonding region of $B_{10}H_{10}^{2-}$.

The next fragment orbital of the first fragment, $1b_1$—the all-bonding combination of the in-plane p orbitals of the ring—actually is of different symmetry in the two interacting fragments (recall the complication mentioned due to the $C_{4v}$ convention). The same is true in the antibonding region MO, for the totally antibonding combination of the perpendicular $p_z$ orbitals of the ring (illustrated at the very top of Figure 4), i.e., in the first fragment this MO is $1b_2$, while in the second it is $1b_1$. There is a good overlap between these ($2b_1$, $2b_2$) and ($1b_1$, $1b_2$) sets, leading to the occupied degenerate $1e_2$ in the $D_{4d}$ symmetry of $B_{10}H_{10}^{2-}$.

The next degenerate set of MOs (2e) gives one bonding ($2e_1$) and one antibonding pair of orbitals. The overlap between the 2e FMOs is very large, so that the out-of-phase combination is pushed above the bonding region of $B_{10}H_{10}^{2-}$. This interaction will prove essential in the sequel in our construction of an electron-counting rule for higher polyhedra. A destabilizing second-order mixing of 1e keeps the bonding combination pretty high, indeed as the HOMO of $B_{10}H_{10}^{2-}$. When all the interactions are accounted for, 11 MOs lie in the bonding region. The overall number is in adherence with Wade's rule, but note that two (not one) of these bonding MOs ($1a_1$ and $1b_2$) are to be characterized as "radial".

We approach $B_{12}H_{12}^{2-}$ similarly, by analyzing the interaction between its two constituent pentagonal pyramids, the *nido*-$B_6H_6^{4-}$ fragments (Figure 5). At this stage, the B−H bonds lie in the $B_5$ plane of their respective pyramid, so that the resultant $B_{12}H_{12}^{2-}$ symmetry is not yet $I_h$, but only $D_{5d}$.

As was the case for $B_{10}H_{10}^{2-}$, interaction between the totally symmetric $1a_1$ radial FMOs leads to two orbitals, both stabilized by the FMO $2a_1$ combinations through second-order interactions. The interaction between the next degenerate $1e_1$ sets leads to two in-phase and out-of-phase combinations, both stabilized by second-order mixing with the $2e_1$ FMOs. The interaction between the $2a_1$ FMOs forms one bonding and one antibonding MO. Both are destabilized by mixing with the low-lying $1a_1$; as a result, the out-of-phase combination is pushed into the antibonding region of $B_{12}H_{12}^{2-}$.

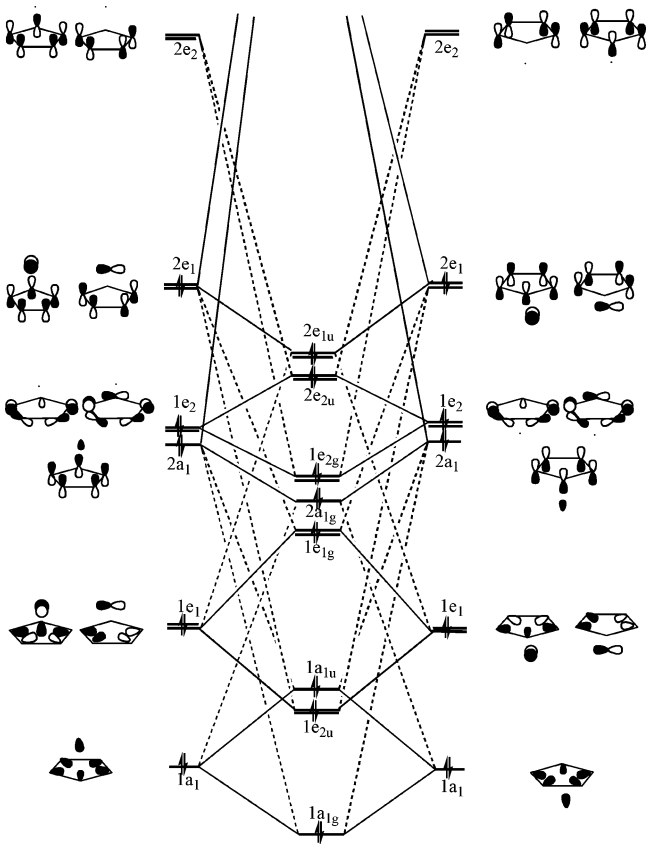


**Figure 5.** The interaction diagram between two *nido*-$B_6H_6^-$ fragments resulting in the bonding MOs of *closo*-$B_{12}H_{12}^{2-}$. Here dashed lines indicate second-order interactions.

So far, the interactions between the FMOs are very similar to what is observed in $B_{10}H_{10}^{2-}$. But unlike the case of $B_{10}H_{10}^{2-}$, the in-plane all-bonding combinations of tangential p orbitals do interact with each other (as they are of the same symmetry, despite the rotation of the second fragment by 36°); they form two in-phase and out-of-phase combinations. Though the splitting is not pronounced, due to the lateral nature of the overlap, second-order mixing from the antibonding region MO $2e_2$ stabilizes both the in-phase and out-of-phase combinations. The next pair of $2e_1$ FMOs of the fragments interacts strongly, forming a pair of bonding and antibonding MOs. Mixing with low-lying $1e_1$ destabilizes both of these MOs. Hence, as in the case of $B_{10}H_{10}^{2-}$, the in-phase combination forms the HOMO.

Though the interaction of orbitals of the four- and five-membered rings used in the above analysis explains the ordering of energy levels, there is a difference in the orientation of ring B−H bonds in the *nido* fragments for $B_{10}H_{10}^{2-}$ and $B_{12}H_{12}^{2-}$ compared to $B_6H_6^{2-}$ and $B_7H_7^{2-}$. The B−H bonds, perforce in the plane of the ring in the case of $B_6H_6^{2-}$ and $B_7H_7^{2-}$, will be bent toward the caps in the case of $B_{10}H_{10}^{2-}$ and $B_{12}H_{12}^{2-}$. In other words, the centroid of the molecule, which lies at the ring center for $B_6H_6^{2-}$ and $B_7H_7^{2-}$, moves to a position between the rings in $B_{10}H_{10}^{2-}$ and $B_{12}H_{12}^{2-}$ (See Figure 6). The bonding and observed

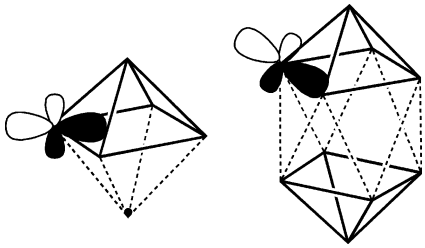

**Figure 6.** Radial and tangential orbitals in building up $B_6H_6^{2-}$ and $B_{10}H_{10}^{2-}$.

geometries of these systems can be more clearly explained if the influence of the geometric perturbation due to this B−H bending is taken into account, as we do in the next section.

## 4. Geometric Perturbation Due to the Bending of B−H Bonds

If one simply were to bring together two $B_5H_5^-$ fragments to form $B_{10}H_{10}^{2-}$, the equatorial B−H bonds in one pyramid would find themselves too close to the B−H bonds of the other. The resultant repulsion presumably leads to the bending of the B−H bonds toward the cap: as much as 19.6°, as observed experimentally. The 6.5° tilt of the B−H bonds of the four-membered ring in $B_5H_5^{4-}$ is far less than the bending here. Let us assume that the sp "out" hybrid at a given boron atom follows the motion of the outer hydrogen. This effectively causes a reorientation of the sp hybrid that points toward the center of the ring (it now points toward the "center" of the polyhedron) as illustrated in Figure 6. One of the tangential orbitals of the ring boron follows the motion, while the other is unaffected.

Let us inquire what will happen to the skeletal orbitals when the B−H bonds, originally in the plane with the ring, bend toward the capping group. The resulting correlation diagram (from an extended Hückel calculation for $B_{10}H_{10}^{2-}$) is depicted in Figure 7. It can be easily seen from Figure 7 that the skeletal orbitals perturbed most by B−H bending are $1e_2$, $1e_1$, $2a_1$, and $2e_2$. While $1e_2$, $2a_1$, and $2e_2$ are stabilized, $1e_1$ is destabilized. The net effect is stabilizing.

We can rationalize this shifting of energy levels from overlap arguments. The FMO overlap (*S*) and FMO overlap population (OP) values between the skeletal MOs of these fragments (see Figure 4) are obtained from extended Hückel calculations by keeping the B−H bonds in the plane of the ring and are given in Table 1 (in parentheses) along with the corresponding values of the optimized geometry.

The $1e_1$ and $1e_2$ orbitals of $B_{10}H_{10}^{2-}$ formed from the 1e FMOs of the *nido*-$B_5H_5$ fragments (see Figure 4) has sp hybrid orbitals of two diagonal boron atoms of the ring. If they follow B−H bending, these hybrids will be redirected toward the cage center and will interact more effectively with the other fragment. Indeed, the overlap between these two FMOs increases from 0.01 to 0.12 (see Table 1) and hence the in-phase combination $1e_2$ is stabilized and the out-of-phase combination $1e_1$ is destabilized (as a function of bending). It can also be seen from Figure 7 that the destabilization of $1e_1$ is more pronounced than the stabilization of $1e_2$, as expected from inclusion of overlap in the calculations.

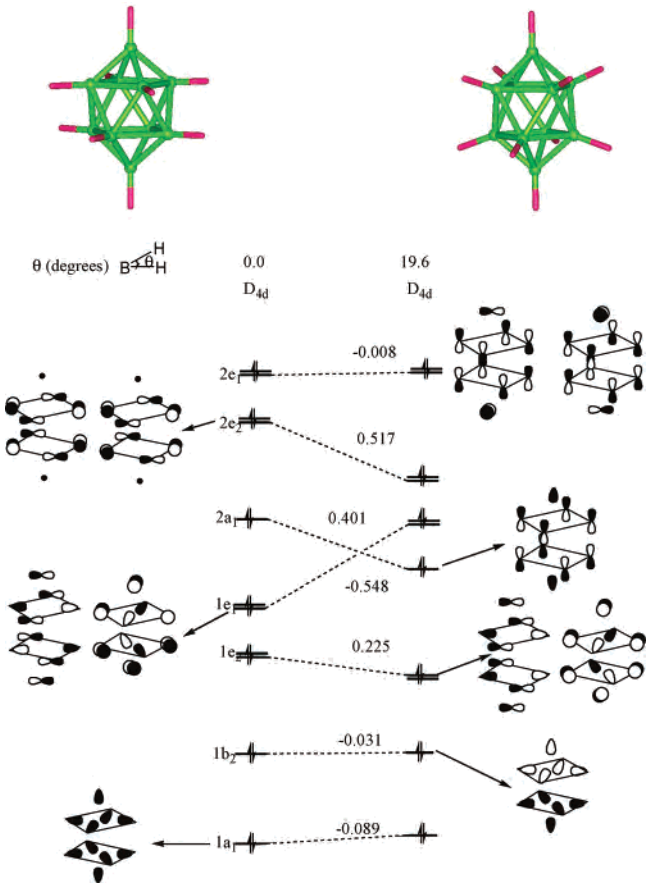


**Figure 7.** A correlation diagram for $B_{10}H_{10}^{2-}$, showing the variation of energy levels (eV) with respect to bending of hydrogens away from the plane of the rings. The vertical energy scale is schematic. The angle $\theta$, specifying the H positions, is defined in the text.

In the case of $2a_1$, which is the bonding combination of FMOs $2a_1$ (Figure 4), the overlap is reduced from 0.28 to 0.25, due to "out-of-plane" B−H bending. The overlap population between these two FMOs follows and is also reduced, from 0.42 to 0.37 (see Table 1). This can be attributed to the "splaying out" of ring tangential $p_z$ orbitals of the fragments as the B−H's move. Surprisingly, Figure 7 shows that this MO is stabilized by B−H bending. Perhaps this is due to the increased overlap between the ring $p_z$ orbitals of the fragments with their respective caps.

MO $2e_2$ is formed from the interaction between the all-bonding combination of the in-plane p orbitals of one fragment and the antibonding region MO that is the out-of-phase combination of the perpendicular $p_z$ orbitals (see Figure 4). The overlap between these fragment orbitals increases from 0.41 to 0.47 as a consequence of B−H bending (see Table 1). Presumably, this change occurs because of the "splaying out" of perpendicular $p_z$ orbitals, increasing their overlap with the in-plane p orbitals which have maximum electron density outside the periphery of the ring. The net overlap population is also substantially increased from 0.36 to 0.45 (see $1b_1$ and $1b_2$ in Figure 4). Thus there is a pronounced stabilization of $2e_2$ MOs due to B−H bending. When all the skeletal MOs of $B_{10}H_{10}^{2-}$ are considered, the net effect of B−H bending is found to be stabilizing.

**Table 1.** FMO Overlap (*S*) and FMO Overlap Population (OP) between Two $B_5H_5^-$ Fragments of $B_{10}H_{10}^{2-}$ (Figure 4), Obtained from Extended Hückel Calculations Using the B3LYP/6-31G* Optimized Geometry[a]

| | $1a_1$ | | 1e | | $2a_1$ | | $1b_1$ | | 2e | |
|---|---|---|---|---|---|---|---|---|---|---|
| MO | OP | *S* | OP | *S* | OP | *S* | OP | *S* | OP | *S* |
| $1a_1$ | −9 (−9) | 19 (16) | | | 4 (0) | 14 (14) | | | | |
| 1e | | | 2 (0) | 12 (1) | | | | | 6 (1) | 24 (15) |
| $2a_1$ | 4 (0) | 14 (14) | | | 37 (42) | 25 (28) | | | | |
| $1b_2$ | | | | | | | | | | |
| 2e | | | 6 (1) | 24 (15) | | | | | 44 (50) | 33 (36) |
| $1b_1$ | | | | | | | 45 (36) | 47 (41) | | |

[a] Numbers inside parentheses correspond to the values when the ring B−H bonds are kept in the plane of the four-membered rings in $B_5H_5^-$ fragments. To avoid decimal points, all the values are multiplied by 100.

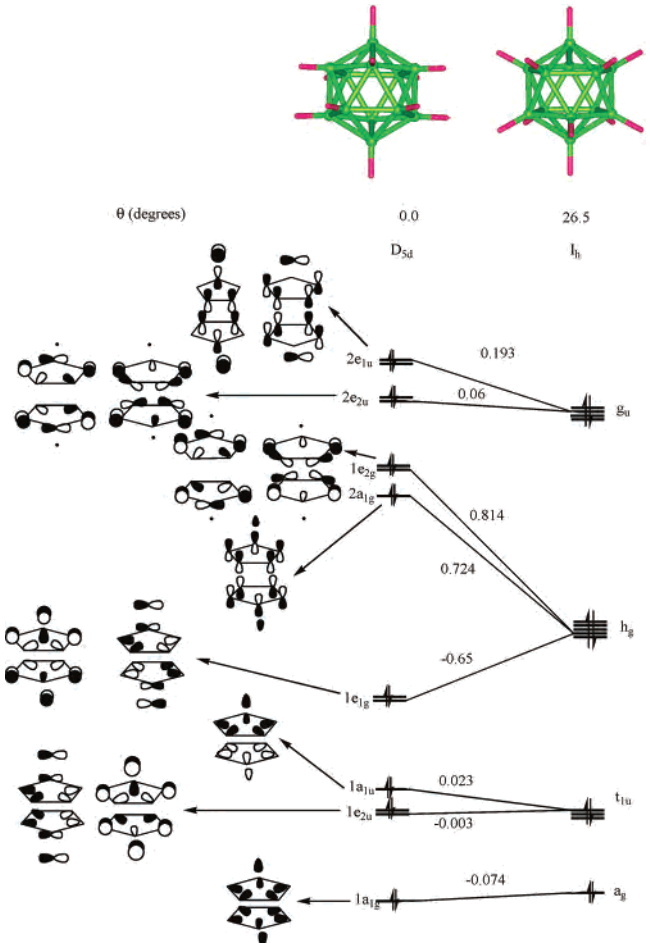


**Figure 8.** A correlation diagram for $B_{12}H_{12}^{2-}$, showing the variation of energy levels (eV) with respect to bending of hydrogens away from the plane of the ring. The vertical energy scale is schematic. The angle $\theta$, specifying the H positions, is defined in the text.

In $B_{12}H_{12}^{2-}$, B−H bonds bend to the inevitable angle ($\theta = 26.5°$) to acquire icosahedral symmetry[15d] (the point group changes from $D_{5d}$ to $I_h$). This is greater by 10.9° than the B−H bending of 15.6° in $B_6H_6^{4-}$ ($C_{5v}$); but this difference is less than in $B_{10}H_{10}^{2-}$. Several MOs then became degenerate as a consequence of the increased symmetry, as illustrated in Figure 8. It is evident from the comparison of Figures 7 and 8 that the B−H bending has more pronounced energy consequences in $B_{12}H_{12}^{2-}$. In analyzing these, we made use of FMO overlap (*S*) and FMO overlap population (OP) values between the skeletal MOs of $B_6H_6^-$ fragments (see Figure 5). These are obtained from extended Hückel calculations by keeping the B−H bonds in the plane of the ring, and are given in Table 2 (within parentheses), along with the corresponding values for the optimized geometry.

The $1e_{2u}$ and $1a_{1u}$ orbitals of $B_{12}H_{12}^{2-}$ ($D_{5d}$) are similar to $1b_2$ and $1e_2$ orbitals of $B_{10}H_{10}^{2-}$, but the icosahedral symmetry forces $t_{1u}$ degeneracy for these three orbitals. Similarly $1e_{1g}$ (analogous to $1e_1$ of $B_{10}H_{10}^{2-}$) is destabilized, as the overlap between the $1e_1$ orbitals of the fragment (Figure 5) increases from 0.10 to 0.22 (Table 2). The $2a_{1g}$ MO of $B_{12}H_{12}^{2-}$, as in the case of $2a_1$ of $B_{10}H_{10}^{2-}$, is stabilized, though the energy changes are more pronounced in $B_{12}H_{12}^{2-}$ than $B_{10}H_{10}^{2-}$. But in the place of all $2e_2$ orbitals of $B_{10}H_{10}^{2-}$, $B_{12}H_{12}^{2-}$ has in-phase ($1e_{2g}$) and out-of-phase ($2e_{2u}$) combinations of in-plane ring p orbitals of the component $B_6H_6^-$ fragment ($1e_2$, see Figure 5), both lying within the bonding region. Though the in-plane p orbitals are not perturbed due to the bending of B−H bonds, both of these degenerate MO pairs $1e_{2g}$ and $2e_{2u}$ are stabilized by B−H bending. This is due to the increased second-order mixing from the antibonding region MO $2e_2$, as in the case of $B_{10}H_{10}^{2-}$.

The overlap between $1e_2$ and $2e_2$ of the fragments is increased from 0.38 to 0.45, and consequently the overlap population is also increased from 0.32 to 0.42 (see Table 2). Unlike the case of $B_{10}H_{10}^{2-}$, the HOMO of $B_{12}H_{12}^{2-}$ ($2e_{1u}$) is also stabilized by B−H bending, as the overlap between the fragments increases from 0.38 to 0.45. The interesting $h_g$ and $g_u$ degeneracies of all these MOs are forced by the icosahedral symmetry of the molecule.

This analysis also helps to understand why the stacking of the rings always occurs in a staggered fashion, forming the deltahedral framework. An eclipsed orientation would not allow effective mixing of perpendicular $p_z$ orbitals with the in-plane ring orbitals; such mixing is essential to the stability of these systems.

There are some subtle differences in the nature of orbital interactions between four- and five-membered-ring stacking. The major difference originates from the $2e_2$ of $B_{10}H_{10}^{2-}$. This orbital arises from the interaction of all-bonding in-plane p orbitals of the *nido*-$B_5H_5^{4-}$ fragment of different symmetry ($1b_1$ and $1b_2$) in the fragment. Stabilization of the $2e_2$ components derives from second-order mixing of an antibonding MO. But in $B_{12}H_{12}^{2-}$, the equivalent orbitals of *nido*-$B_6H_6^{4-}$ ($1e_2$) do interact, giving a pair of in-phase and out-of-phase combinations, both of which are stabilized by second-order mixing from antibonding $2e_2$ orbitals of the fragment.

**Table 2.** MO Overlap (*S*) and FMO Overlap Population (OP) between Two $B_6H_6^-$ Fragments of $B_{12}H_{12}^{2-}$ (Figure 5), Obtained from Extended Hückel Calculations Using the B3LYP/6-31G* Optimized Geometry[a]

| | $1a_1$ | | $1e_1$ | | $2a_1$ | | $1e_2$ | | $2e_1$ | |
|---|---|---|---|---|---|---|---|---|---|---|
| MO | OP | *S* | OP | *S* | OP | *S* | OP | *S* | OP | *S* |
| $1a_1$ | −12 (−14) | 22 (20) | | | 6 (1) | 13 (14) | | | | |
| $1e_1$ | | | −2 (−2) | 22 (10) | | | | | 10 (1) | 21 (16) |
| $2a_1$ | 6 (1) | 13 (14) | | | 35 (40) | 25 (26) | | | | |
| $1e_2$ | | | | | | | −1 (0) | 13 (1) | | |
| $2e_1$ | | | 10 (1) | 21 (16) | | | | | 37 (50) | 29 (35) |
| $2e_2$ | | | | | | | 42 (32) | 45 (38) | | |

[a] Numbers inside parentheses correspond to the values when the ring B−H bonds are kept in the plane of the five-membered ring in $B_6H_6^-$ fragments. To avoid decimal points, all the values are multiplied by 100.

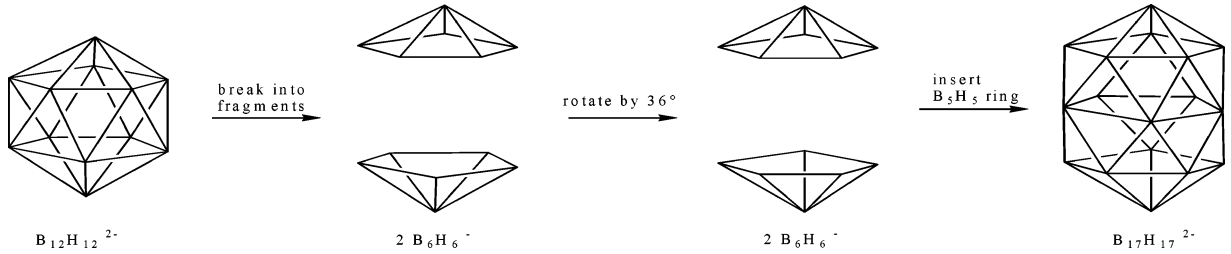


**Figure 9.** Conceptual construction of $B_{17}H_{17}^{2-}$ from $B_{12}H_{12}^{2-}$ by the insertion of a $B_5H_5$ ring.

Taken as a whole, the interaction between $B_6H_6^-$ fragments is more pronounced than that of $B_5H_5^-$. In both the cases, the three MOs (a + e) arising from the set of perpendicular $p_z$ orbitals of the ring are primarily responsible for ring−ring bonding. This is reflected in higher OP values corresponding to these MOs as given in Tables 1 and 2. The highest OP values are found for the e set of one fragment interacting with the in-plane MOs of the other. The out-of-phase combinations of the a + e MOs are pushed to the antibonding region. These interactions are more pronounced in $B_{12}H_{12}^{2-}$ than in $B_{10}H_{10}^{2-}$.

All other BMOs arise out of nonbonding or destabilizing four-electron−two-orbital interactions, though many of them are stabilized by the second-order mixing from the higher lying MOs of appropriate symmetry. This is well reflected in the group-OP values. Even when the ring hydrogens are kept in the plane of the ring, the group-OP between the nido fragments in $B_{12}H_{12}^{2-}$ is 1.60, whereas in $B_{10}H_{10}^{2-}$ it is only 1.50. The bending of the ring B−H bonds toward their cap causes a further increase in the group-OP values, and is more pronounced in $B_{12}H_{12}^{2-}$ (2.56) than $B_{10}H_{10}^{2-}$ (2.08). This shows up in the greater distance between the rings in $B_{10}H_{10}^{2-}$ in comparison with $B_{12}H_{12}^{2-}$ (see Figure 1). Interaction between the nido fragments (taken now as $B_6H_6^-$ and $B_5H_5^-$) results in a net stabilization of 3.55 eV in $B_{12}H_{12}^{2-}$, whereas it is only 3.40 eV in $B_{10}H_{10}^{2-}$. It can be concluded that staggered stacking of five-membered rings is more favorable than that of the four-membered rings. The dominant contribution to interfragment bonding from the MOs composed of $p_z$ orbitals at the ring atoms will lead us to an easy way of deducing favored electron counts for higher boranes.

## 5. Extended Stacking

Stacking of staggered rings can be extended, in principle leading to borane nanotubes.[18,20] Conceptually, insertion of one more five-membered $B_5H_5$ ring into the icosahedral $B_{12}H_{12}^{2-}$ (Figure 9) leads to $B_{17}H_{17}^{2-}$ with $D_{5h}$ symmetry, which is a minimum on its potential energy surface at the B3LYP/6-31G* level of theory.[11] The next members in the series will be $B_{22}H_{22}^{2-}$, $B_{27}H_{27}^{2-}$, etc. The number and nature of bonding molecular orbitals for these mini-nanotubes can be easily deduced. As seen in the previous section, the MOs arising from the perpendicular $p_z$ orbitals of the ring interact particularly strongly. Thus to begin with, we will restrict our attention to this set of three MOs and the effect of stacking on them, for the sake of building up electron-counting principles.

In an aufbau, any member of the series can be generated from its predecessor by the insertion of an *arachno*-$B_5H_5$ (charge unspecified as yet) planar five-membered ring. For illustration, let us analyze *closo*-$B_{17}H_{17}^{2-}$. This molecule can be conceptually formed by breaking $B_{12}H_{12}^{2-}$ into two *nido*-$B_6H_6$ ($C_{5v}$) fragments and inserting a $B_5H_5$ ($D_{5h}$) ring between them (charge not yet specified) in such a way that all the adjacent five-membered rings are in a staggered orientation. This is shown schematically in Figure 9. Before the insertion of the planar $B_5H_5$ ring, one of the *nido*-$B_6H_6$ fragments has to be rotated through the $C_5$ axis by 36° with respect to the other.

Each of the "broken" *nido*-$B_6H_6$ ($C_{5v}$) fragments requires ($n$ + 2) electron pairs by Wade's rule and hence would carry a −4 charge by itself.[4] The frontier BMOs of *nido*-$B_6H_6^{4-}$ are similar to the $\pi$ orbitals of a cyclopentadienyl. The MOs we are interested in are those arising from the perpendicular $p_z$ orbitals of the open face. They correspond to the $2a_1$ and $2e_1$ MOs discussed earlier in Figure 5, and will be referred to hereafter as a and e. The $B_5H_5$ ($D_{5h}$) fragment, also like

(20) (a) Derecskei-Kovacs, A.; Dunlap, B. I.; Lipscomb, W. N.; Lowrey, A.; Marynick, D. S.; Massa, L. *Inorg. Chem.* **1994**, *33*, 5617. (b) Quong, A. A.; Pederson, M. R.; Broughton, J. Q. *Phys. Rev. B* **1994**, *50*, 4787. (c) Tang, A.; Li, Q.; Liu, C.; Li, J. *Chem. Phys. Lett.* **1993**, *201*, 465. (d) Fowler, P. W.; Lazzeretti, P.; Zanasi, R. *Inorg. Chem.* **1988**, *27*, 1298.

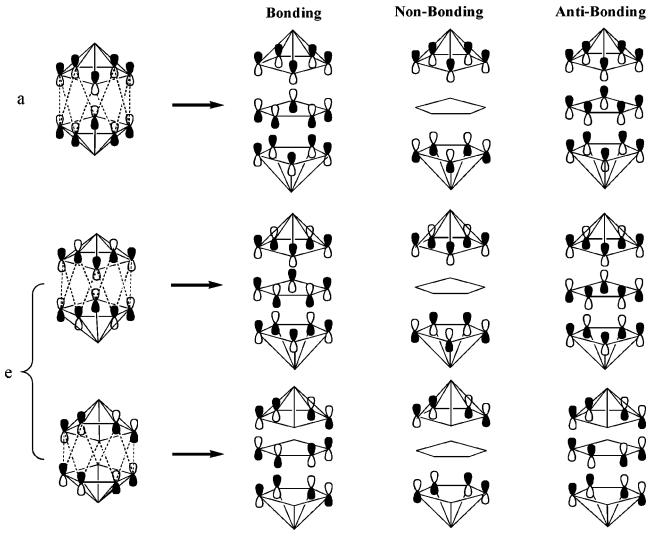


**Figure 10.** The molecular orbitals arising from the perpendicular $p_z$ orbitals by the insertion of a $B_5H_5$ ring between two $B_6H_6$ fragments in $B_{12}H_{12}^{2-}$.

cyclopentadienyl, has three BMOs of a and e symmetry and will have a −6 charge if those levels are filled ($B_5H_5^{6-}$ is like $C_5H_5^-$).

When the $B_5H_5^{6-}$ ring is inserted between the two *nido*-$B_6H_6^{4-}$ ($C_{5v}$) fragments, the MOs from different fragments will interact. There arise typical three-orbital interactions, each of the a and e sets generating a bonding, a nonbonding, and an antibonding combination, as illustrated in Figure 10. All the levels (nine of them) are filled for the starting point of ($2B_6H_6^{4-} + B_5H_5^{6-}$). But to maximize the bonding, by analogy to smaller *closo*-borane dianions, one should only fill the bonding combinations, i.e., a total of three levels in Figure 10. This results in a −2 charge, or $B_{17}H_{17}^{2-}$ ($2B_6H_6^{4-} + B_5H_5^{6-} \rightarrow B_{17}H_{17}^{14-} \rightarrow B_{17}H_{17}^{2-} + 12e^-$. An extended Hückel calculation on $B_{17}H_{17}^{2-}$ with B−B distances kept 1.79 Å shows a large HOMO−LUMO gap (4.70 eV), confirming the above conclusion. Hence Wade's $n + 1$ formula still holds good. Similar interactions and arguments are found in the stacking of three-membered-ring $(Pt_3(CO)_6)_n$ fragments, for which chains with $n$ as large as 10 are experimentally characterized, all of them as dianions.[19]

Note that the nonbonding combinations (third column in Figure 10) are not filled on stacking. This is because there are BMOs of the same symmetry below these MOs, which interact with these combinations and destabilize them. For example, of the three occupied radial BMOs for $B_{17}H_{17}^{2-}$ shown in Figure 11, the $a_1'$ orbital mixes with the lowest nonbonding combination of the $p_z$ set. The same mixing of course leads to stabilization of the radial orbital of the system, as shown in Figure 12.

Earlier in this paper, we gave an argument for preferring "staggering" to "eclipsing" in $B_{12}H_{12}^{2-}$. This is also true for the higher nanotubes, which prefer the triangulation that comes from staggering each ring relative to its neighbors.

DFT calculations carried out at the B3LYP/6-31G* level of theory on $B_{17}H_{17}^{2-}$ indicate that the B−B bonds of the center ring are elongated substantially,[11a] to 2.127 Å. This is the import of dashed lines in Figure 1: the deltahedral framework is, in a way, broken; while there is bonding within

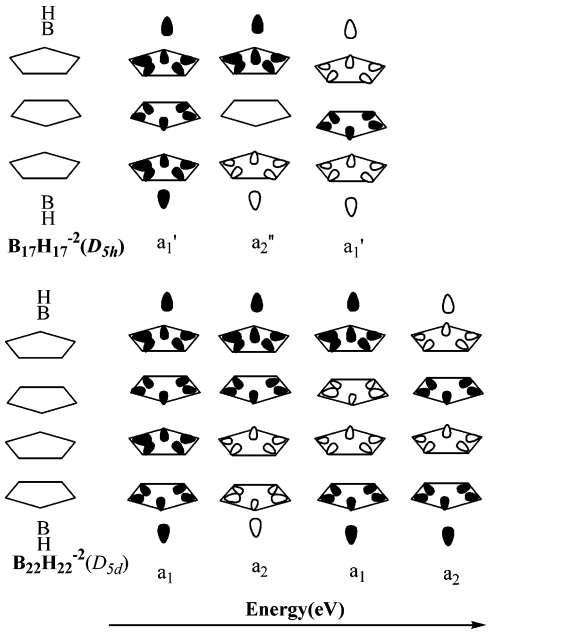


**Figure 11.** The radial bonding molecular orbitals of $B_{17}H_{17}^{2-}$ and $B_{22}H_{22}^{2-}$.

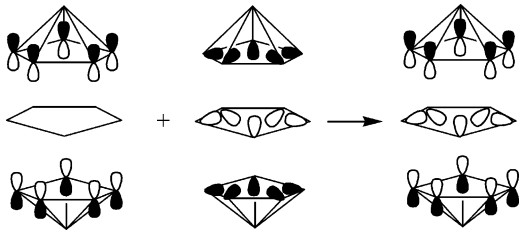

**Figure 12.** The mixing of the nonbonding $p_z$ MO with the radial BMO in $B_{17}H_{17}^{2-}$.

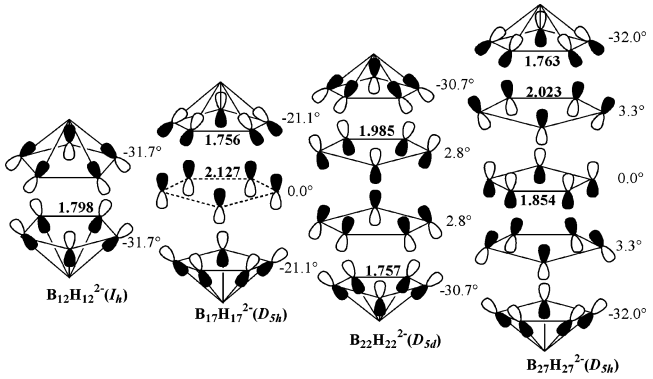


**Figure 13.** Reorientation of perpendicular $p_z$ orbitals in borane nanotubes is illustrated for the most bonding MO made up of $p_z$ orbitals. The bending of B−H bonds from the plane of the ring is given alongside the rings. The values near the bonds are calculated B−B distances in Å.

the center ring, it is not clear if one should draw a full "bond line" there. Why does this happen? As noticed earlier, due to the B−H bending in the $B_6H_6$ fragment toward the capping B−H group, the "perpendicular" $p_z$ orbitals of the $B_6H_6$ fragment will be splayed away from the center on the other side of the cap. The "splaying-out" of $p_z$ orbitals in borane nanotubes is illustrated schematically for one BMO in Figure 13. In $B_{17}H_{17}^{2-}$ expansion of the center ring makes for more effective overlap with the $B_6H_6$ fragment $p_z$ orbitals. Calculations show that the group overlap between the central $B_5H_5$

ring with the two *nido*-$B_6H_6$ fragments increases from 4.03 to 5.72 as a result of the center ring expansion. This offers a plausible explanation for the long B−B distances in the central ring. It can also be seen from Figure 13 that the bending of B−H bonds toward the cap is decreased when compared with $B_{12}H_{12}^{2-}$. We can say that all these geometry changes are the result of the molecule optimizing cap/center ring group overlaps.

Despite the expansion of the central ring, $B_{17}H_{17}^{2-}$ is predicted to be the most stable among *closo* boranes by B−H increment schemes and highly aromatic by NICS based assessments.[11a] Isolobal substitution of the B−H group with other groups having more diffuse orbitals such as $^{+}$SiH, Fe(Cp), etc. will improve the overlap and may help in the experimental characterization of this skeleton.

Insertion of one more ring in a similar way leads to *closo*-$B_{22}H_{22}^{2-}$. The argument for the 2− magic electron count is similar to the one given above. The radial BMOs of this species are given in Figure 11. As in the case of $B_{17}H_{17}^{2-}$, some of these orbitals will be stabilized by the MOs composed of the perpendicular $p_z$ orbitals of appropriate symmetry. The optimized geometry at the B3LYP/6-31G* level indicates that in this molecule the B−B bonds of the central ring (1.985 Å) are significantly reduced compared to $B_{17}H_{17}^{2-}$ (2.127 Å). One might expect that the B−H bonds of the central rings should be bent toward the terminal ring to avoid steric interactions. But in the optimized geometry they are bent in the opposite direction, i.e., toward each other. This is in accord with our hypothesis that the $p_z$ orbitals of the central rings are also splayed out a little to maximize the overlap with the terminal rings (Figure 13). To maximize overlap with the $B_6H_6$ groups, the central ring B−B distance is now reduced.

The next member of the series, $B_{27}H_{27}^{2-}$ is also found to have reduced ring elongation (in comparison with $B_{17}H_{17}^{2-}$) at the same level of theory. Here the B−B bonds of the central five-membered ring shrink to 1.854 Å, since the $p_z$ orbitals of its adjacent rings are splayed "in" toward the center of the molecule (Figure 13). Frequency calculations are consistent with the bond length trends. These mini-nanotubes are alternatively fat and thin along the tube axis.

It follows by induction that insertion of every additional ring between a ring and cap also will generate similar interactions and lead to a −2 charge. Effectively there are just three such MOs that are bonding between the rings, irrespective of the number of rings in the system. But the optimized geometry has reasonably short B−B distances along the minitube (Figure 1). Obviously there must be more than six electrons contributing to the bonding along the minitubes. These must come from orbitals other than these three tangential $p_z$ BMOs. Indeed some locally radial orbitals contribute to bonding along the minitube, by the second-order mixing mechanism described earlier for $B_{17}H_{17}^{2-}$.

## 6. Conclusion

We have studied the effect of staggered stacking of boron rings that leads to a deltahedral skeleton for tubular $B_nH_n^{2-}$. Apart from giving an argument for the abundance of icosahedral and octahedral structures in boron-rich borides, these perturbation theory based studies also point out that five-membered-ring stacking intrinsically involves more pronounced stabilization than stacking of four-membered rings. With the increase in the number of rings, second-order interactions are increasingly responsible for ring−ring bonding. The widely believed explanation that the *closo* boranes have one radial orbital and *n* tangential orbitals is found to be misleading, even for well-known $B_{10}H_{10}^{2-}$ and $B_{12}H_{12}^{2-}$. Nevertheless, Wade's $n + 1$ rule, as a formula, is found to be applicable even for extended borane nanotubes (although it is claimed to be inapplicable[20] in higher spherical systems such as icosahedral $B_{32}H_{32}$). In Wade's rule we have a case of a beautiful regularity, remarkably productive in rationalizing and predicting real chemistry. That the reasons for its applicability (the radial/tangential partitioning) fail to be met for some cases—the tubular boranes from $B_{10}H_{10}^{2-}$ on—does not at all detract from the value of this rule.

**Acknowledgment.** M.M.B. and R.H. gratefully acknowledge the support of the National Science Foundation (CHE-99-700089 and CHE-02-04841). E.D.J. and P.D.P. acknowledge the CSIR, India, for their support.

**Supporting Information Available:** Optimized Cartesian coordinates of various borane nanotubes and their total energies. This material is available free of charge via the Internet at http://pubs.acs.org.

IC0262435